## **Time-Crystalline Topological Superconductors**

Aaron Chew<sup>®</sup>, David F. Mross<sup>®</sup>, and Jason Alicea<sup>®</sup><sup>1,3</sup>

<sup>1</sup>Department of Physics and Institute for Quantum Information and Matter, California Institute of Technology, Pasadena, California 91125, USA

<sup>2</sup>Department of Condensed Matter Physics, Weizmann Institute of Science, Rehovot 76100, Israel <sup>3</sup>Walter Burke Institute for Theoretical Physics, California Institute of Technology, Pasadena, California 91125, USA

(Received 8 August 2019; accepted 31 January 2020; published 5 March 2020)

Time crystals form when arbitrary physical states of a periodically driven system spontaneously break discrete time-translation symmetry. We introduce one-dimensional time-crystalline topological superconductors, for which time-translation symmetry breaking and topological physics intertwine—yielding anomalous Floquet Majorana modes that are not possible in free-fermion systems. Such a phase exhibits a bulk magnetization that returns to its original form after two drive periods, together with Majorana end modes that recover their initial form only after four drive periods. We propose experimental implementations and detection schemes for this new state.

DOI: 10.1103/PhysRevLett.124.096802

Introduction.—Periodically driven quantum systems evade certain constraints imposed in equilibrium. For instance, "time crystals" that spontaneously break time-translation symmetry in the sense envisioned in Refs. [1,2] cannot arise in equilibrium [3], yet can emerge with periodic driving. In periodically driven time crystals any physical (i.e., noncat) state evolves with a subharmonic of the drive frequency [4–6]. The canonical realization consists of disordered Ising spins that collectively flip after each drive period, thereby requiring two periods to recover their initial state. Experiments have detected signatures of time crystallinity both in driven cold atoms [7,8] and solid-state spin systems [9–11].

As a second, deeply related example, consider a onedimensional (1D) free-fermion topological superconductor hosting Majorana end modes [12], each described by a Hermitian operator  $\gamma$ . If  $\gamma$  adds energy E then  $\gamma^{\dagger}$  adds -E, while Hermiticity requires that these be equivalent. In equilibrium the unique solution is E = 0—corresponding to the well-studied Majorana zero modes. Periodically driving with frequency  $\Omega$  additionally permits "Floquet Majorana modes" carrying  $E = \Omega/2$  since energy is then only conserved mod  $\Omega$  [13]. Floquet Majorana modes have been proposed to facilitate more efficient quantum information processing compared to equilibrium systems [14-16]. Moreover, they encode a topological flavor of time-translation symmetry breaking in that Floquet Majorana operators change sign each drive cycle, thus also requiring two periods to recover their initial form.

We merge the phenomena above by exploring periodically driven 1D topological superconductors generated upon coupling Cooper-paired electrons to doubled-periodicity time-crystalline Ising spins. Such "time-crystalline topological superconductors" intertwine bulk time-translation

symmetry breaking and topological physics—yielding anomalous quadrupled-periodicity Floquet Majorana modes that categorically cannot arise in free-fermion platforms. We propose implementation via quantum-dot arrays (see Fig. 1) reminiscent of setups utilized in Refs. [17–19] for engineering equilibrium Majorana zero modes. We derive and analyze an exactly solvable, physically intuitive model for time-crystalline topological superconductivity and show that probing junctions between time-crystalline and static topological superconductors reveals the Floquet Majorana modes' quadrupled periodicity.

Model and setup.—Time-crystalline topological superconductors closely relate to equilibrium topological superconductors that spontaneously violate electronic time-reversal symmetry  $\mathcal{T}$ , which importantly satisfies  $\mathcal{T}^2 = -1$ . We thus begin by modeling the latter. Our setup,

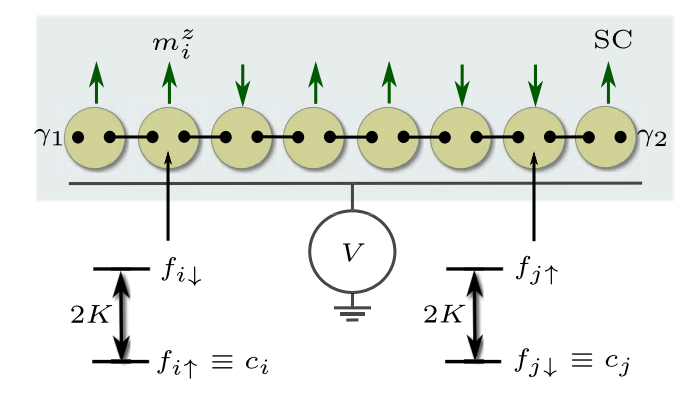


FIG. 1. Proximitized quantum-dot array coupled to Ising spins. The Ising spins polarize the dot electrons—effectively producing a system of spinless fermions  $c_j$ . In any Ising configuration, the fermions can realize topological superconductivity with unpaired Majorana zero modes  $\gamma_{1,2}$  that intertwine with the adjacent spins.

sketched in Fig. 1, consists of a superconductor coupled to a chain of quantum dots indexed by sites j, each hosting one active spinful level described by operators  $f_{j\sigma}$  ( $\sigma=\uparrow,\downarrow$  denotes spin, which we implicitly sum over whenever suppressed); we assume that charging energy is quenched by coupling to the superconductor and can thus be neglected. A chain of Ising spins described by Pauli matrices  $m_j^z$  resides proximate to the quantum-dot array. We model the setup with a  $\mathcal{T}$ -symmetric Hamiltonian  $H=H_0+H_f$ , where

$$H_0 = \sum_{i} \left( -J m_j^z m_{j+1}^z - K m_j^z f_j^{\dagger} \sigma^z f_j \right), \tag{1}$$

$$\begin{split} H_f &= \sum_j [-\mu f_j^\dagger f_j - t (f_j^\dagger f_{j+1} + \text{H.c.}) \\ &+ \alpha (i f_j^\dagger \sigma^x f_{j+1} + \text{H.c.}) + \Delta (f_{j\uparrow} f_{j\downarrow} + \text{H.c.})]. \end{split} \tag{2}$$

In  $H_0$ , J > 0 ferromagnetically couples neighboring Ising spins and K > 0 couples the Ising and dot spins. Terms in  $H_f$  describe the chemical potential  $(\mu)$ , hopping (t), spin-orbit coupling  $(\alpha)$ , and proximity-induced pairing  $(\Delta)$  for the quantum-dot electrons.

Suppose that the *K* term dominates and energetically enforces alignment of each electron spin with the nearest Ising spin. Only one of the two spinful levels in each dot remains active at low energies—effectively creating a system of spinless fermions described by operators

$$c_{j} = \frac{1}{2} [(1 + m_{j}^{z}) f_{j\uparrow} + (1 - m_{j}^{z}) f_{j\downarrow}], \tag{3}$$

as Fig. 1 illustrates. Time-reversal  $\mathcal{T}$  sends  $m_j^z \to -m_j^z$  and  $c_j \to m_j^z c_j$ , thus satisfying time-reversal symmetry. This intertwinement between spinless fermions and Ising spins is unavoidable; without it,  $c_j$  has no way of acquiring the required minus sign upon two applications of  $\mathcal{T}$ .

In the Supplemental Material [20], we project *H* onto the spinless-fermion subspace by integrating out high-energy fermionic modes, yielding an effective Hamiltonian

$$H_{\text{eff}} = \sum_{j} [-Jm_{j}^{z}m_{j+1}^{z} - \mu'c_{j}^{\dagger}c_{j} + (t'_{m_{j}^{z},m_{j+1}^{z}}c_{j}^{\dagger}c_{j+1} + \Delta'_{m_{j}^{z},m_{j+1}^{z}}c_{j}c_{j+1} + \text{H.c.})].$$
 (4)

Here  $\mu'=-(K+\mu)$  is a renormalized chemical potential, while  $t'_{m_j^z,m_{j+1}^z}=a+a^*m_j^zm_{j+1}^z$  and  $\Delta'_{m_j^z,m_{j+1}^z}=bm_j^z-b^*m_{j+1}^z$  denote Ising-spin-dependent effective hopping and p-wave pairing amplitudes, with  $a=(-t+i\alpha)/2$  and  $b=(-t+i\alpha)\Delta/(K-\mu)$ . The real part of a sets the hopping strength between sites with aligned Ising spins, which is directly inherited from spin-conserving tunneling in Eq. (2); the imaginary part similarly fixes the hopping when Ising spins antialign, which is instead mediated by

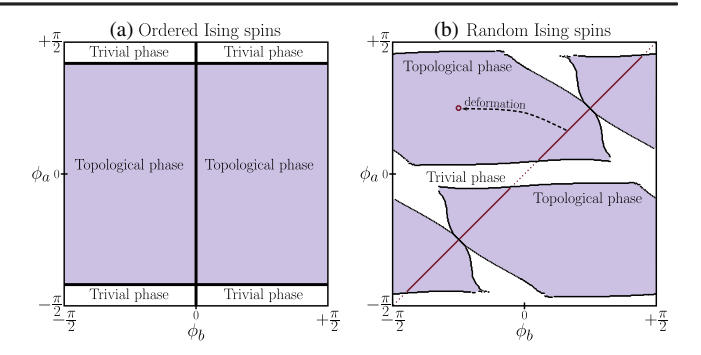


FIG. 2. Phase diagram for Eq. (4) assuming (a) fully polarized and (b) random Ising spins. In (a) a nonzero chemical potential  $\mu' = |a|$  generates the trivial phase, and the system is gapless along the thick black lines. Data in (b) were generated from transfer-matrix simulations at  $\mu' = |b| = |a|/4$  with  $10^6$  sites. Data points indicate sharp peaks in the localization length, as expected at a topological phase transition. The red diagonal line  $\phi_a = \phi_b$  is relevant for the physical quantum-dot setup from Fig. 1. As the dashed arrow illustrates, the topological phase along this line can be deformed to the zero-correlation-length limit with  $\phi_a = \pi/4$ ,  $\phi_b = -\pi/4$  (and also |a| = |b|,  $\mu' = 0$ ) without crossing a phase boundary. Increasing the magnitude of  $\mu'$  tends to thicken the trivial regions, while altering the relative magnitudes of |a| and |b| shifts the boundaries separating the topological and trivial phases.

spin-orbit coupling  $\alpha$ . Pairing in  $H_{\rm eff}$  follows from second-order processes that involve virtual excitations out of the spinless-fermion subspace—hence the  $K-\mu$  energy denominator in b. Depending on the Ising configuration, either spin-conserving hopping or spin-orbit coupling virtually creates a doubly occupied site of f fermions that then Cooper pair via the original s-wave  $\Delta$  term, effectively mediating p-wave pairing of spinless fermions.

Phase diagram.—Equation (4) describes a strongly interacting system of Ising spins and fermions. Nevertheless, for any given Ising configuration the model reduces to free fermions. Consider first uniformly polarized all-up or all-down Ising spins. Here Eq. (4) maps to the familiar Kitaev chain [12] with uniform hopping strength  $2|a|\cos\phi_a$  and pairing  $\pm 2i|b|\sin\phi_b$ , where  $a=|a|e^{i\phi_a}$  and  $b=|b|e^{i\phi_b}$ . (Our derivation above yielded  $\phi_a=\phi_b$ , though it will be useful to now keep these phases independent.) Accordingly, the chain hosts edge Majorana zero modes provided the chemical potential intersects the band and pairing is finite, i.e., for  $|\mu'| < 4|a| |\cos\phi_a|$  and  $\sin\phi_b \neq 0$  as sketched in Fig. 2(a).

To examine the fermionic ground state with random Ising spins—which is our main interest—we compute the correlation length  $\xi$  using the transfer-matrix technique; see, e.g, Ref. [21] and the Supplemental Material [20]. This method allows us to map out phase boundaries by numerically searching for diverging  $\xi$  as we vary  $\phi_{a,b}$ ; for our purposes a regular  $400 \times 400$  grid of  $\phi_a$  and  $\phi_b$  values in the interval  $[-\pi/2, \pi/2]$  is sufficient. [Exploiting

 $\xi(\phi_a,\phi_b)=\xi(-\phi_a,-\phi_b)$  halves the number of simulations]. Figure 2(b) illustrates representative results obtained for  $\mu'=|b|=|a|/4$  and  $N=10^6$  sites. The data points indicate local maxima where  $\xi$  is typically of order  $10^2$  or larger, while it is of order unity elsewhere. We expect these peaks to represent true divergences in  $\xi$  when  $\phi_a$  or  $\phi_b$  are tuned continuously in the thermodynamic limit. Topological regions are easily identified via exact diagonalization on smaller systems and confirming the presence of edge Majorana zero modes. In the Supplemental Material we analytically capture the topological phase for a restricted window of  $\phi_{a,b}$  via the Born approximation.

For our quantum-dot setup, we expect  $\phi_a = \phi_b$  [red line in Fig. 2(b)] and also  $|a| \gg |b|$  since p-wave pairing encoded in b appears at second order in perturbation theory. Starting from the topological phase in this physical regime, Fig. 2(b) strongly suggests that we can deform parameters to  $\phi_a = \pi/4$  and  $\phi_b = -\pi/4$ , |a| = |b|, and  $\mu' = 0$  without encountering a divergent  $\xi$ . (See the Supplemental Material [20] for additional evidence.) This special point corresponds to the model's zero-correlation-length limit. Here it is convenient to decompose the spinless fermions in terms of Majorana operators  $\eta_{A,Bj}$  via  $c_j = e^{-i(\pi/4)m_j^z}(\eta_{Bj} + i\eta_{Aj})$ , whereupon Eq. (4) becomes

$$H'_{\text{eff}} = \sum_{j} (-J m_{j}^{z} m_{j+1}^{z} - i \kappa s_{m_{j}^{z}, m_{j+1}^{z}} \eta_{Aj} \eta_{Bj+1}), \quad (5)$$

with  $s_{m_i,m_j} = (1-m_i+m_j+m_im_j)/2 = \pm 1$  and  $\kappa = 4\sqrt{2}|a|$ . For any choice of  $m_j^z$ s the Majorana operators dimerize nontrivially as shown in Fig. 1, yielding Majorana zero modes

$$\gamma_1 \equiv \eta_{B1} = e^{i(\pi/4)m_1^z}c_1 + \text{H.c.},$$

$$\gamma_2 \equiv \eta_{AN} = -ie^{i(\pi/4)m_N^z}c_N + \text{H.c.},$$
(6)

at the leftmost and rightmost sites. Notice the spin-fermion intertwinement inherent in the zero modes, which consequently evolve under  $\mathcal T$  via

$$\gamma_1 \to m_1^z \gamma_1, \qquad \gamma_2 \to -m_N^z \gamma_2,$$
(7)

again consistent with  $\mathcal{T}^2=-1$ . All Hamiltonian eigenstates are at least fourfold degenerate in this limit: one factor of 2 arises because  $\mathcal{T}$  flips all Ising spins, while the other reflects topological degeneracy encoded in the Majorana zero modes. The topological degeneracy of the fermionic ground states given a static Ising configuration persists even away from the special limit examined above, due to the finite gap for fermionic excitations. Moreover, the Supplemental Material [20] shows that Eq. (7) holds even when the zero-mode wave functions extend over many sites.

Adiabatic cycle.—Next we generalize Eq. (1) to

$$H_0' = \sum_{j} [-J(\hat{\mathbf{n}} \cdot \mathbf{m}_j)(\hat{\mathbf{n}} \cdot \mathbf{m}_{j+1}) - K(\hat{\mathbf{n}} \cdot \mathbf{m}_j) f_j^{\dagger} \hat{\mathbf{n}} \cdot \boldsymbol{\sigma} f_j],$$
(8)

where  $\mathbf{m}$ ,  $\boldsymbol{\sigma}$  denote vectors of Pauli matrices and the unit vector  $\hat{\mathbf{n}} \equiv \cos\theta \hat{\mathbf{z}} + \sin\theta \hat{\mathbf{y}}$  determines the easy axis for the Ising spins. At either  $\theta = 0$  or  $\pi$ ,  $H_0'$  reduces to Eq. (1). Suppose that we again deform to the zero-correlation-length limit (which is possible for any  $\theta$ ) and then implement the following cycle: (i) start with an arbitrary Ising spin configuration at  $\theta = 0$ , (ii) initialize the fermions into one of the topological-superconductor ground states, and finally (iii) adiabatically rotate the easy axis by winding  $\theta$  from 0 to  $\pi$ .

Although the Hamiltonian returns to its original form, the wave functions do not. Rather, the cycle slowly rotates all Ising spins by  $\pi$ , while the fermions follow their instantaneous minimum-energy configuration given the adiabaticity. The initial ground state thereby transforms into its time-reversed counterpart. One rotation sends  $m_j^z \rightarrow -m_j^z$ ,  $f_j \rightarrow e^{i(\pi/2)\sigma^x}f_j$ , and hence  $c_j \rightarrow ic_j$ . Majorana zero modes thus transform as  $\gamma_1 \rightarrow m_1^z \gamma_1$  and  $\gamma_2 \rightarrow m_N^z \gamma_2$ , similar to the action of  $\mathcal{T}$ . Interestingly, two cycles return the Ising spins to their original form whereas four cycles are required to recover the initial zero-mode operators, e.g.,

$$\gamma_1 \to m_1^z \gamma_1 \to -\gamma_1 \to -m_1^z \gamma_1 \to \gamma_1.$$
 (9)

Time-crystalline topological superconductivity and detection.—We now promote the adiabatic ground-state phenomenon described above to a dynamic phenomenon applicable to arbitrary physical states. To this end we apply a variation of the preceding cycle periodically with period T, thus generating time-crystalline topological superconductivity. We specifically consider a binary drive such that the Floquet operator that evolves the system over a single period reads

$$U_T = e^{-i(\pi/2 - \epsilon) \sum_j (m_j^x + c_j^\dagger c_j)} e^{-iTH_{\text{eff}}^{\text{dis}}}.$$
 (10)

The right exponential evolves the system with respect to a disordered, static Hamiltonian  $H_{\rm eff}^{\rm dis}$  that is the same as Eq. (4) but with J, a, b replaced with random site-dependent couplings  $J_j$ ,  $a_j$ ,  $b_j$ . We neglect randomness in the phases of  $a_j$ ,  $b_j$  and treat  $J_j$ ,  $a_j$ ,  $b_j$  as independent random variables with magnitudes drawn from uniform distributions  $[\bar{J}-\delta J,\bar{J}+\delta J],[\bar{a}-\delta a,\bar{a}+\delta a],[\bar{b}-\delta b,\bar{b}+\delta b]$ . Disorder crucially introduces many-body localization (MBL) into the dynamics and prevents heating to infinite temperatures [22–26]. The left exponential in Eq. (10) performs an instantaneous "kick" that (at least approximately) flips the Ising spins via a transverse magnetic field

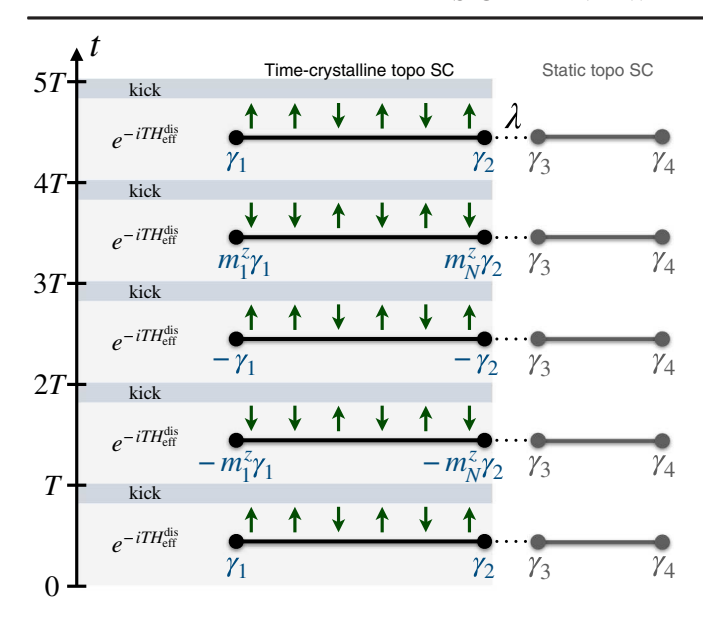


FIG. 3. Time evolution for the time-crystalline topological superconductor generated by Eq. (10) at  $\epsilon=0$ . Each period T globally flips all Ising spins, yielding doubled-periodicity bulk response, whereas the Floquet Majorana modes  $\gamma_{1,2}$  exhibit quadrupled-periodicity response that can be probed in the junction with the static topological superconductor on the right. The inner Majorana modes  $\gamma_{2,3}$  hybridize with coupling strength  $\lambda$ . Since  $\gamma_3$  is static while  $\gamma_2$  evolves nontrivially after each period T, the junction's energy inherits the latter's quadrupled periodicity.

pulse and applies a potential to the spinless fermions—thereby mimicking evolution from our adiabatic cycle without the adiabaticity requirement.

The dynamics is analytically tractable at  $\epsilon=0$  and when  $H_{\rm eff}^{\rm dis}$  reduces to Eq. (5) with random couplings  $J_j, \kappa_j$ . Starting from any Ising configuration, the "perfect" kick in  $U_T$  sends  $m_j^z \to -m_j^z$  and thus flips all spins, signifying period-doubling time crystallinity in the spin sector. In the fermionic sector,  $\gamma_{1,2}$  in Eq. (6) continue to commute with  $H_{\rm eff}^{\rm dis}$  despite the randomness. The kick, however, nontrivially transforms the Majorana edge operators so that  $U_T\gamma_1U_T^\dagger=m_1^z\gamma_1$  and  $U_T\gamma_2U_T^\dagger=m_N^z\gamma_2$ . Precisely as illustrated in Eq. (9),  $\gamma_{1,2}$  therefore require four drive periods to recover their initial form, i.e., they form the hallmark quadrupled-periodicity Floquet Majorana modes. Shaded regions of Fig. 3 summarize the evolution.

Quadrupled periodicity can be experimentally probed in junctions between time-crystalline and static topological superconductors as in the right side of Fig. 3, wherein  $\gamma_3$  and  $\gamma_4$  denote time-independent Majorana zero modes. Electron tunneling across the junction couples  $\gamma_2$  with  $\gamma_3$ , producing a Hamiltonian term  $H_{23} = i\lambda\gamma_2\gamma_3$  for some  $\lambda$  that may depend on the adjacent Ising spins. Consequently, the junction's energy density (among other local properties) directly manifests the quadrupled-periodicity built into the anomalous Floquet Majorana mode  $\gamma_2$ .

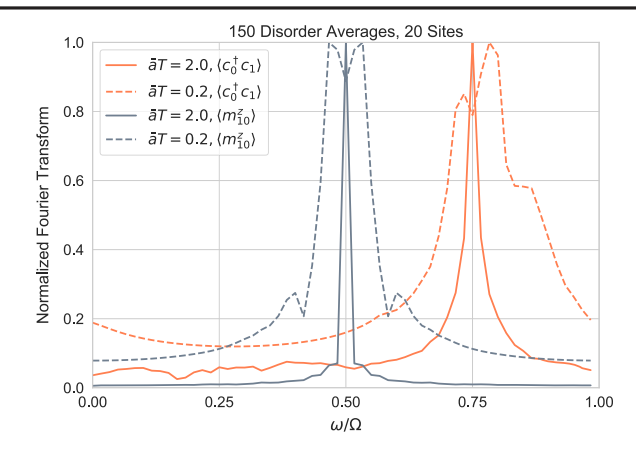


FIG. 4. Fourier transform of the quantities shown in the legend following time evolution via Eq. (10) with  $\epsilon = 0.2$  and parameters specified in the main text. Data are normalized by setting the maximum of each Fourier spectrum to 1, and frequency  $\omega$  on the horizontal axis is normalized by  $\Omega = 2\pi/T$ , with T the drive period. Here  $m_{10}^z$  represents an Ising spin at the center of the chain,  $c_0$  is an auxiliary zero-energy static fermion that enables probing the Floquet Majorana mode periodicity, and  $c_1$  is the fermion at the left end of the quantum-dot chain. For initialization we use random Ising configurations and random fermionic states that entangle  $c_0$  with the rest of the system. Runs were repeated 150 times for disorder averaging with maximum bond dimension  $\chi = 50$ ; similar results were obtained with  $\chi = 25$ . For  $\bar{a}T = 2$ sharp peaks persist at  $\Omega/2$  and  $3\Omega/4$ —despite "imperfect" driving generated by  $\epsilon \neq 0$ —indicating "rigid" doubled-periodicity Ising spins and quadrupled-periodicity Floquet Majorana modes characteristic of time-crystalline topological superconductivity. For  $\bar{a}T = 0.2$ , the imperfect drive pushes the peak frequencies away from these quantized values, indicating a loss of rigid time crystallinity.

Rigidity against "imperfect" drives is a crucial feature of time-crystalline phases [4–6,27]. Here, such imperfection arises from taking  $\epsilon \neq 0$  and  $H_{\rm eff}^{\rm dis}$  away from the zero-correlation-length limit, which spoils exact solvability and prompts us to turn to numerics.

Numerics.—We employ time-evolving block decimation (TEBD), using a maximum bond dimension of  $\chi = 50$ , on a 20-site system with random Ising spins and parameters appropriate for our quantum-dot setup:  $\phi_a = \phi_b = \pi/8$ ,  $\bar{b} = \bar{a}/2, \ \bar{J} = \bar{a}/4, \ \mu' = 0, \ \delta a = \delta b = \delta J = \bar{a}/8.$  Our simulations incorporate a decoupled, static zero-energy fermion  $c_0$  that functions similarly to the static topological superconductor in Fig. 3. We initialize into a state that entangles the static fermion with the rest of the system. We then simulate the Floquet operator in Eq. (10) with  $\bar{a}T=2$ and  $\bar{a}T = 0.2$ , and with the kick shifted away from commensurability by  $\epsilon = 0.2$  [28]. Despite the rather small system size, in both cases the bond dimension quickly saturated, and the truncation error was relatively coarse. To check robustness of our numerics we repeated the computations for maximum bond dimension  $\chi = 25$ , and the results agreed with those at  $\chi = 50$ .

Over a run of 60 Floquet evolutions and 150 disorder averages, we measure the Ising spin  $\langle m_{i=10}^z \rangle$  in the middle of the system as well as  $\langle c_0^{\dagger} c_1 \rangle$ , where  $c_1$  corresponds to the leftmost quantum dot. The former probes bulk time crystallinity while the latter probes the Floquet Majorana modes. Figure 4 plots the Fourier transform of both quantities as a function of frequency  $\omega$  normalized by  $\Omega = 2\pi/T$ . For  $\bar{a}T = 2$  the data show the rigidity characteristic of a time crystal: despite the imperfect drive, the bulk magnetization and edge fermion bilinear, respectively, remain peaked at  $\omega = \Omega/2$  and  $\omega = 3\Omega/4$  (as expected for doubled-periodicity Ising spins and quadrupled periodicity Floquet Majorana modes). By contrast, in our  $\bar{a}T = 0.2$ simulations both peaks clearly shift due to nonzero  $\epsilon$ , indicating an absence of rigid time-crystallinity for this case. We also ran exact numerics on a seven-site system and measured the level-spacing statistics of the  $U_T$  eigenvalues. At  $\bar{a}T = 2$  the mean level spacing was approximately 0.39, close to the Poisson value 0.386 expected for MBL [29].

Discussion.—The admixture of symmetry breaking and topology is known to generate new physics in static systems; examples include  $8\pi$ -periodic Josephson effects [30,31] and enrichment of Majorana braiding and fusion [32]. Our work establishes that driven systems can be similarly enriched by "decorating" topological phases with spontaneous time-translation symmetry breaking. We specifically showed that 1D time-crystalline topological superconductors engineered from quantum-dot arrays host novel Floquet Majorana modes that display anomalously long periodicity not possible with free fermions. Exotic states of this type are not captured by the cohomology classification of interacting topological Floquet phases [33–37]. Our work opens up the possibility of harnessing time crystals to enrich other "designer" phases of matter. One could envision promoting spinless fermions to spinful fermions coupled to magnetic degrees of freedom in systems such as driven spinless 2D p + ip superconductors [38–40]. Subtleties regarding MBL in two dimensions can be avoided by focusing on prethermal regimes, possibly leading to new higher-dimensional adiabatic cycles and time-crystalline topological phases.

It is a pleasure to thank David Weld and Norm Yao for illuminating discussions. This work was supported by the Army Research Office under Grant No. W911NF-17-1-0323; the NSF through Grant No. DMR-1723367; Grant No. 2016258 from the United States-Israel Binational Science Foundation (BSF); the Israel Science Foundation (ISF); the Caltech Institute for Quantum Information and Matter, an NSF Physics Frontiers Center with support of the Gordon and Betty Moore Foundation through Grant No. GBMF1250; the Walter Burke Institute for Theoretical Physics at Caltech; and the Gordon and Betty Moore Foundation's EPiQS Initiative, Grant No. GBMF8682 to J. A.

- [1] F. Wilczek, Phys. Rev. Lett. 109, 160401 (2012).
- [2] A. Shapere and F. Wilczek, Phys. Rev. Lett. 109, 160402 (2012).
- [3] H. Watanabe and M. Oshikawa, Phys. Rev. Lett. 114, 251603 (2015).
- [4] V. Khemani, A. Lazarides, R. Moessner, and S. L. Sondhi, Phys. Rev. Lett. 116, 250401 (2016).
- [5] D. V. Else, B. Bauer, and C. Nayak, Phys. Rev. Lett. 117, 090402 (2016).
- [6] N. Y. Yao, A. C. Potter, I.-D. Potirniche, and A. Vishwanath, Phys. Rev. Lett. 118, 030401 (2017).
- [7] J. Zhang, P. W. Hess, A. Kyprianidis, P. Becker, A. Lee, J. Smith, G. Pagano, I.-D. Potirniche, A. C. Potter, A. Vishwanath, N. Y. Yao, and C. Monroe, Nature (London) 543, 217 (2017).
- [8] J. Smits, L. Liao, H. T. C. Stoof, and P. van der Straten, Phys. Rev. Lett. 121, 185301 (2018).
- [9] S. Choi, J. Choi, R. Landig, G. Kucsko, H. Zhou, J. Isoya, F. Jelezko, S. Onoda, H. Sumiya, V. Khemani, C. von Keyserlingk, N. Y. Yao, E. Demler, and M. D. Lukin, Nature (London) 543, 221 (2017).
- [10] S. Pal, N. Nishad, T. S. Mahesh, and G. J. Sreejith, Phys. Rev. Lett. 120, 180602 (2018).
- [11] J. Rovny, R. L. Blum, and S. E. Barrett, Phys. Rev. Lett. 120, 180603 (2018).
- [12] A. Y. Kitaev, Phys. Usp. 44, 131 (2001).
- [13] L. Jiang, T. Kitagawa, J. Alicea, A. R. Akhmerov, D. Pekker, G. Refael, J. I. Cirac, E. Demler, M. D. Lukin, and P. Zoller, Phys. Rev. Lett. 106, 220402 (2011).
- [14] R. W. Bomantara and J. Gong, Phys. Rev. Lett. 120, 230405 (2018).
- [15] R. W. Bomantara and J. Gong, Phys. Rev. B 98, 165421 (2018).
- [16] B. Bauer, T. Pereg-Barnea, T. Karzig, M.-T. Rieder, G. Refael, E. Berg, and Y. Oreg, Phys. Rev. B 100, 041102 (2019).
- [17] T.-P. Choy, J. M. Edge, A. R. Akhmerov, and C. W. J. Beenakker, Phys. Rev. B 84, 195442 (2011).
- [18] J. D. Sau and S. D. Sarma, Nat. Commun. 3, 964 (2012).
- [19] I. C. Fulga, A. Haim, A. R. Akhmerov, and Y. Oreg, New J. Phys. 15, 045020 (2013).
- [20] See the Supplemental Material at http://link.aps.org/ supplemental/10.1103/PhysRevLett.124.096802 for additional details about the effective Hamiltonian, transfer matrix and Born approximation calculations, and the symmetry properties of anomalous Majorana modes.
- [21] A. MacKinnon, Transfer matrices and disordered systems, in Anderson Localization and Its Ramifications: Disorder, Phase Coherence and Electron Correlations, edited by T. Brandes and S. Kettemann (Springer Berlin Heidelberg, Berlin, Heidelberg, 2003), pp. 21–30.
- [22] D. A. Huse, R. Nandkishore, V. Oganesyan, A. Pal, and S. L. Sondhi, Phys. Rev. B 88, 014206 (2013).
- [23] A. Lazarides, A. Das, and R. Moessner, Phys. Rev. E **90**, 012110 (2014).
- [24] L. D'Alessio and M. Rigol, Phys. Rev. X 4, 041048 (2014).
- [25] P. Ponte, Z. Papić, F. Huveneers, and D. A. Abanin, Phys. Rev. Lett. **114**, 140401 (2015).
- [26] D. A. Abanin, W. D. Roeck, and F. Huveneers, Ann. Phys. (Amsterdam) **372**, 1 (2016).

- [27] C. W. von Keyserlingk, V. Khemani, and S. L. Sondhi, Phys. Rev. B 94, 085112 (2016).
- [28] Calculations were performed using the ITensor Library, http://itensor.org.
- [29] A. Pal and D. A. Huse, Phys. Rev. B 82, 174411 (2010).
- [30] F. Zhang and C. L. Kane, Phys. Rev. Lett. 113, 036401 (2014).
- [31] C. P. Orth, R. P. Tiwari, T. Meng, and T. L. Schmidt, Phys. Rev. B **91**, 081406(R) (2015).
- [32] A. Chew, D. F. Mross, and J. Alicea, Phys. Rev. B **98**, 085143 (2018).
- [33] D. V. Else and C. Nayak, Phys. Rev. B **93**, 201103(R) (2016).

- [34] A. C. Potter, T. Morimoto, and A. Vishwanath, Phys. Rev. X 6, 041001 (2016).
- [35] C. W. von Keyserlingk and S. L. Sondhi, Phys. Rev. B 93, 245145 (2016).
- [36] R. Roy and F. Harper, Phys. Rev. B 94, 125105 (2016).
- [37] R. Roy and F. Harper, Phys. Rev. B 95, 195128 (2017).
- [38] Z. bo Wang, H. Jiang, H. Liu, and X. Xie, Solid State Commun. **215–216**, 18 (2015).
- [39] X. Yang, B. Huang, and Z. Wang, Sci. Rep. **8**, 2243 (2018).
- [40] D. T. Liu, J. Shabani, and A. Mitra, Phys. Rev. B 99, 094303 (2019).